Li *et al. Robot. Biomim.* (2016) 3:11
DOI 10.1186/s40638-016-0045-z

Robotics and Biomimetics

RESEARCH Open Access

Energy-efficient control of a screw-drive pipe robot with consideration of actuator's characteristics

Peng Li[1,2*], Shugen Ma[3,4], Congyi Lyu[2], Xin Jiang[1] and Yunhui Liu[2]

Abstract

Pipe robots can perform inspection tasks to alleviate the damage caused by the pipe problems. Usually, the pipe robots carry batteries or use a power cable draining power from a vehicle that has many equipments for exploration. Nevertheless, the energy is limited for the whole inspection task and cannot keep the inspection time too long. In this paper, we use the total input energy as the cost function and a more accurate DC motor model to generate an optimal energy-efficient velocity control for a screw-drive pipe robot to make use of the limited energy in field environment. We also propose a velocity selection strategy that includes the actual velocity capacity of the motor, according to the velocity ratio k_v, to keep the robot working in safe region and decrease the energy dissipation. This selection strategy considers three situations of the velocity ratio k_v and has a wide range of application. Simulations are conducted to compare the proposed method with the sinusoidal control and loss minimization control (minimization of copper losses of the motor), and results are discussed in this paper.

Keywords: In-pipe robot, Energy-efficient control, Optimal velocity strategy

Background

With the advancement of the robotics and industrial technology, many pipe robots have been developed to explore the pipes that have cracks or defects to avoid serious accidents [1–4].

Up to now, there are more focus on the energy-efficient control of robots [5, 6]. Robots that perform pipe inspection task are often in the field environment, and the energy is a crucial limitation to the time of execution of a task. Most of the pipe robots are driven by DC motors. If the energy-efficient method is applied to the pipe inspection system, the energy dissipation will be decreased and the total time of performing a task will be increased. The energy dissipated through many ways, but only controlling the armature current and field current losses is feasible [7, 8]; further, many researchers conducted on the loss minimization control of the DC motor [9, 10]. They use the armature resistance loss and field resistance loss as the performance index to reduce the energy dissipation, and get the optimal control law, but in the view of the total input energy that is drawn from the power source is usually not optimal.

This paper proposes an energy-efficient solution for the control of a screw-type pipe robot by using an improved DC motor model and employing the total input energy as the performance index that reflect the whole system energy consumption. Straight pipe structure is the most common type; thus, this paper is limited to discuss the condition that the pipe robot is used in the straight horizontal pipe. Additionally, sinusoidal fashion control and the loss minimization control that only considers armature resistance are used as the comparison methods.

Methods

The screw-drive pipe robot

The environment of the pipe is not invariable; thus, the pipe robot should possess the characteristics of multi-function, adaptability and efficiency. The screw-drive

*Correspondence: lipeng.bird@gmail.com
[1] School of Mechanical Engineering and Automation, Harbin Institute of Technology Shenzhen Graduate School, ShenZhen 518055, China
Full list of author information is available at the end of the article

robots are not rare [3, 4], and driving principle is illustrated in Fig. 1.

Typical screw-drive robot is usually composed of a rotator, elastic support arms, rollers and a motor for driving. The rollers have a constant incline angle with respect to the cross section of the pipe. When the motor turns, the whole body moves forward. If the motor turns reversely, the body moves backward. To propel a screw-drive-type robot, one motor is enough for straight pipe and elbow. However, for the T-shape pipe, extra navigation mechanism is needed.

A screw-type robot considered in this paper is shown in Fig. 2a. The advantage of this robot is that it has mobile ability in the pipe and detecting function for inspection, while only one DC motor is installed, which results in low energy consumption and low cost to fabricate. The robot has two working modes: a driving mode and a detecting mode. The robot propels itself in the pipe under the driving mode, and it is used for finding the defect of the pipe under the detecting mode. By setting an on–off solenoid, the two working modes will switch to each other; thus, the robot performs the inspection task without other extra motors. Therefore, such a robot is an efficient design, because it uses one motor and a solenoid to perform a task instead of two motors (one motor for moving and the other motor for detecting). There are two types of driving arm: One type has a constant incline angle as shown in Fig. 1b, while the incline angle of the other type changes according to the payload variation. The two types of driving arm can be both fixed on the robot, but this paper only considers the driving arms with constant incline angle. Further detailed information, for example, the mechanical structure, can be found in [4].

Motion equation of the DC motor

Basic equations of the DC motor

An armature-controlled DC motor is shown in Fig. 3, in which the field current is constant.

The basic equations of circuit are

$$L_a \frac{di_a}{dt} + R_a i_a + V_b = V_a \tag{1}$$

$$i_a = i_m + i_h \tag{2}$$

L_a is the armature inductance (the voltage generated by L_a is much smaller than that of R_a and V_b; thus, in this paper we do not consider the influence of L_a, V_a and V_b is the applied armature voltage and back-emf, respectively. R_a is the armature resistance, while R_h is equivalent resistance for power losses due to the air resistance of rotor and power loss due to the friction between mechanical parts, and Ma had pointed out that the R_h should be included when the motor efficiency is calculated [11]. i_a, i_h and i_m are the current of the R_a, R_h and the armature, respectively. And the back-emf V_b and the armature torque and current are given by

$$V_b = K_e \omega_m \tag{3}$$

$$T_m = K_t i_m \tag{4}$$

$$i_m = i_a - V_b / R_h \tag{5}$$

where K_e and K_t is the back-emf constant and torque constant, respectively, and they have the same value, when SI units are used.

By using the above equation, we can also calculate the value of R_h,

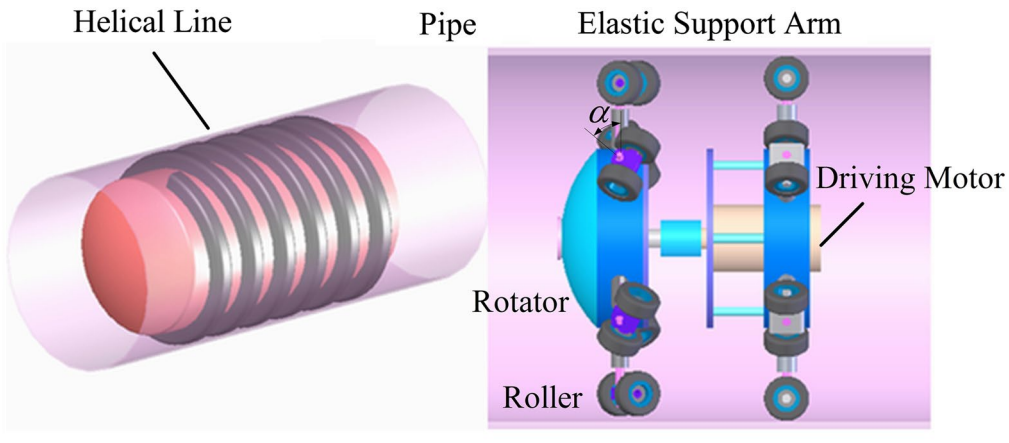

Fig. 1 The screw-type pipe robot. **a** Sketch of the driving principle, **b** typical screw-drive-type robot

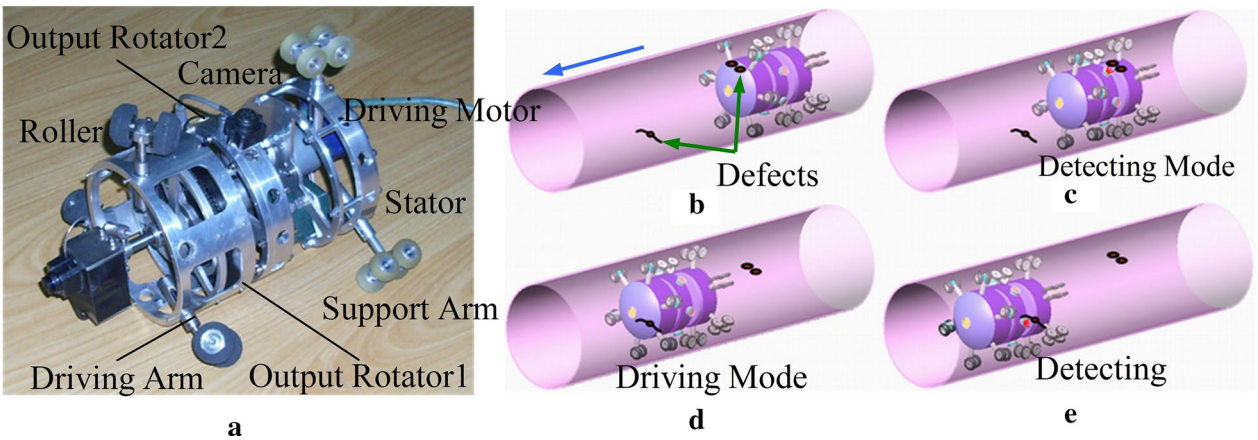

Fig. 2 The screw-drive robot with driving and detecting ability with one DC motor. **a** Prototype, **b** robot is under driving mode, **c** the solenoid is electrified, and robot is under detecting mode and check the defect of the pipe, **d** after checking the area, the solenoid is set off, and the robot is back to driving mode again, **e** another operation cycle of detecting

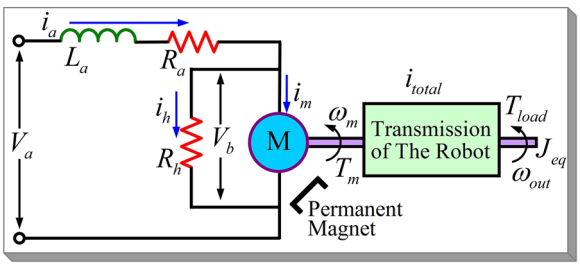

Fig. 3 Equivalent circuit of the DC motor

$$R_{\mathrm{h}} = \frac{V_{\mathrm{b}}}{i_{\mathrm{a}} - i_{\mathrm{m}}} = \frac{K_{\mathrm{e}}\omega_{\mathrm{m}}R_{\mathrm{a}}}{V_{\mathrm{b}} - K_{\mathrm{e}}\omega_{\mathrm{m}} - R_{\mathrm{a}}i_{\mathrm{m}}} \tag{6}$$

As shown in Fig. 3, the whole robot has been treated as a power transmission with a gear ratio of i_{total}; as a result, it amplify the motor torque T_{m} and angular velocity ω_{m} into that of the output rotator T_{out} and ω_{out} and conquer the payload T_{load}. Thus, the dynamics of the motor is

$$J_{\mathrm{eq}}\frac{\mathrm{d}\omega_{\mathrm{m}}}{\mathrm{d}t} + c_{\mathrm{m}}\omega_{\mathrm{m}} + \frac{T_{\mathrm{load}}}{i_{\mathrm{total}}} = T_{\mathrm{m}} \tag{7}$$

c_{m} is the viscous coefficient of the motor, and T_{load}, J_{eq} are the load torque and equivalent moment of inertia of the robot's output rotator and the rotor of the motor, respectively.

Efficiency of the DC motor

From the above equations, the mechanical power generated by the motor is $T_{\mathrm{m}}\omega_{\mathrm{m}}$, and the motor efficiency η_{motor} is

$$\eta_{\mathrm{motor}} = \frac{T_{\mathrm{m}}\omega_{\mathrm{m}}}{V_{\mathrm{a}}i_{\mathrm{a}}} \tag{8}$$

The above equations have shown the influence of R_{h}, when calculating the motor efficiency. Moreover, using the above equations, the motor efficiency that is considering R_{a} and R_{h} and that of only considering R_{a} is shown in Fig. 4 with the same parameters in Table 1. The reason of Fig. 4's result is that considering R_{a} and R_{h} needs more electrical energy than that of only considering R_{a}, when the motor working at a same combination of torque and velocity. The motor efficiency has decreased, when R_{h} is considered.

Motion and force analysis of the robot

The kinematics of the wheel-type robot is generally calculated by

$$v = \omega_{\mathrm{out}}\gamma \tag{9}$$

while v and ω_{out} are the translational speed and rotational speed of robot, respectively. γ, here, is a coefficient that converts rotational speed into translational speed. Moreover, the kinematics of screw-drive robot is (detailed can be found in [3, 4])

$$\begin{aligned} v &= \omega_{\mathrm{out}}(r_{\mathrm{w}} + L)\tan\alpha \\ \gamma &= (r_{\mathrm{w}} + L)\tan\alpha \end{aligned} \tag{10}$$

r_{w} is the radius of the roller and $L = 0.5D - r_{\mathrm{w}}$, while D is the inner diameter of the pipe; α is the constant incline angle, as shown in Fig. 5.

Let F_{dj} and F_{rj} denote the normal and tangential friction, and f_{n} and f_{t} be the corresponding frictional coefficients, respectively. F_{re} is all the other resistant forces acting on the robot, and n is the number of the driving arms. The static equilibrium equations can be derived from Fig. 5

$$n\left(F_{dj}\cos\alpha - F_{rj}\sin\alpha\right) = F_{\mathrm{re}} \tag{11}$$

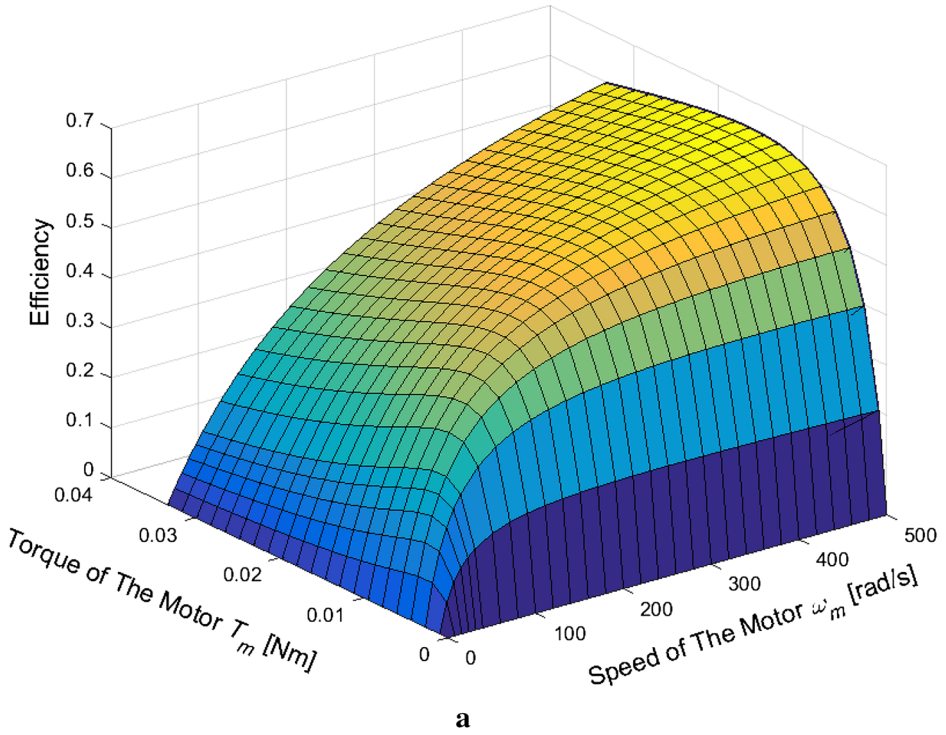

a

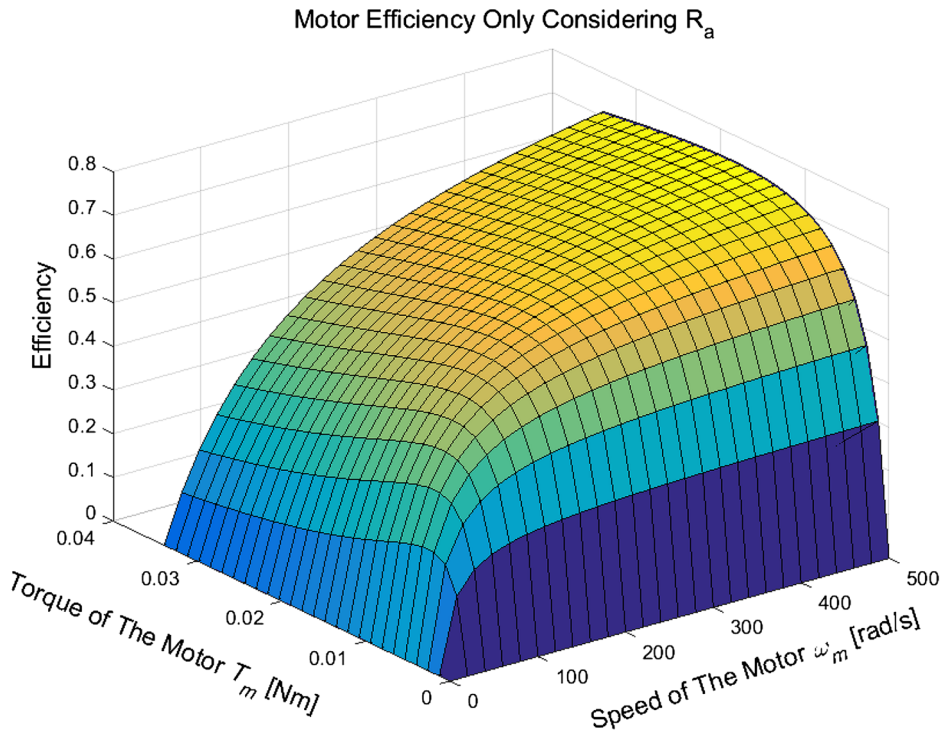

b

Fig. 4 Efficiency of an armature-controlled DC motor. **a** Motor efficiency that considering R_a and R_h, **b** motor efficiency that only considering R_a

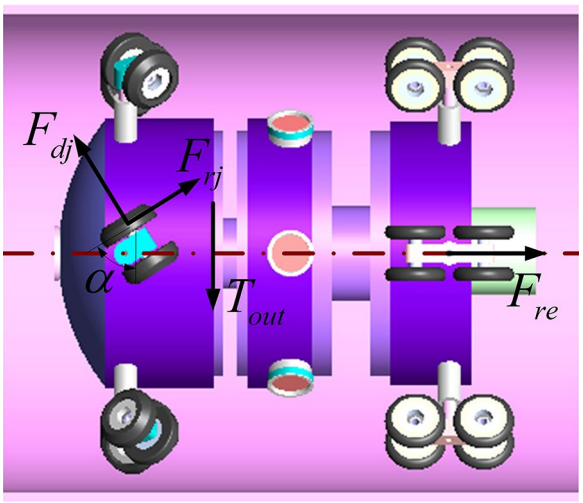

Fig. 5 Forces acting on the robot

$$n\left(F_{dj}\sin\alpha + F_{rj}\cos\alpha\right) = 2T_{\text{out}}/D \tag{12}$$

From (11)and (12), the relation between T_{load} and T_{out} is

$$T_{\text{load}} = \frac{F_{dj}\cos\alpha - F_{rj}\sin\alpha}{F_{dj}\sin\alpha + F_{rj}\cos\alpha}T_{\text{out}} = F(\alpha)T_{\text{out}} \tag{13}$$

Thus, the load torque term $T_{\text{load}}/i_{\text{total}}$ can be updated by $T_{\text{load}}/F(\alpha)i_{\text{total}}$. Now, we consider the condition of not including the tangential friction force. Figure 6a, b shows the value of $F(\alpha)$ with environment parameters $f_{\text{n}} = 0.5$ and $f_{\text{t}} = 0.01$ and that of $f_{\text{n}} = 0.5$ and $f_{\text{t}} = 0$. As shown in Fig. 6c, the difference of the two conditions is almost the same after an artificial coefficient 0.91 multiplies $F(\alpha)$ between 9° and 20°, under the condition $f_{\text{n}} = 0.5$ and $f_{\text{t}} = 0$.

Now, $F(\alpha)$ can be simplified as follows

$$F(\alpha) = 0.91\cot\alpha \tag{14}$$

while the 0.91 is the artificial coefficient to calculate $F(\alpha)$ between the angle of 9° and 20°. The motion equation is derived

$$J_{\text{eq}}\dot{\omega}_{\text{m}} + \left(\frac{K_{\text{t}}K_{\text{e}}}{R_{\text{h}}} + c_{\text{m}}\right)\omega_{\text{m}} + \frac{T_{\text{load}}}{i_{\text{total}}F(\alpha)} - K_{\text{t}}i_{\text{a}} = 0 \tag{15}$$

and the state equation is given by

$$\dot{\omega}_{\text{m}} = -A\omega_{\text{m}} + Bi_{\text{a}} + C \tag{16}$$

where $A = \frac{K_{\text{t}}K_{\text{e}}+c_{\text{m}}R_{\text{h}}}{J_{\text{eq}}R_{\text{h}}}$, $B = \frac{K_{\text{t}}}{J_{\text{eq}}}$, $C = -\frac{T_{\text{load}}}{F(\alpha)J_{\text{eq}}i_{\text{total}}}$.

Energy-efficient control

According to the task requirements, this robot has two modes:

1. Cruise start/stop mode: Cruise start mode is used to start the motor and the robot at a specified speed; then, the motor and the robot keep this speed moving to find the potential defect of the pipe. When the detecting camera finds the suspicious defect, the robot will stop and detect that area carefully; thus, stopping the robot is called cruise stop mode.
2. Location mode: Sometimes, a segment of pipe need not to be checked; thus, the robot just passes by. The operator only inputs the displacement S_{f} within the time t_{f}; then, the optimal velocity profile is generated according to the value of k_{v}, which is a speed ratio defined in (38).

Cruise start/stop mode

Under this mode, the final velocity ω_{f} and the corresponding time t_{f} are given, and the optimal velocity profile is generated by the control law. After the time t_{f}, the actuator of the robot will keep the value of ω_{f} moving forward, since keeping the velocity invariant will result in the minimization of the extra consumption of the total input electrical energy. On the contrary, under the cruise

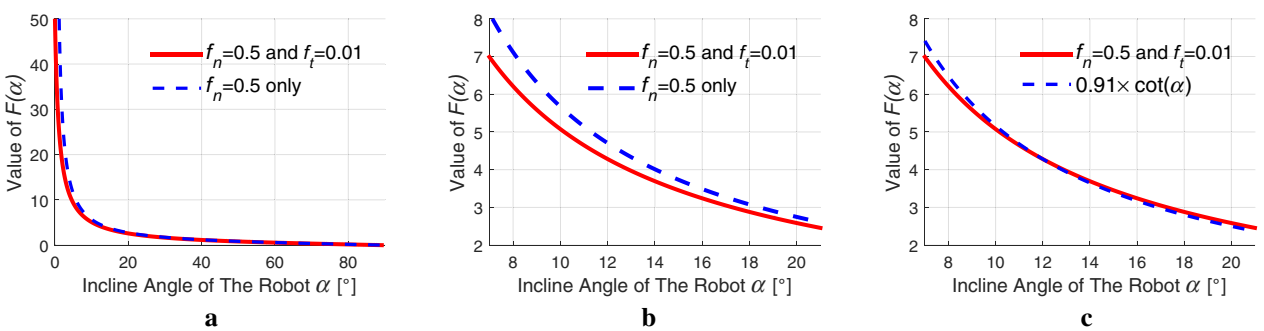

Fig. 6 Values of $F(\alpha)$. **a** $f_n = 0.5$ and $f_t = 0.01$ versus $f_n = 0.5$ only. **b** Zoom in figure of (**a**) with the interval from 8° to 20°. **c** $f_n = 0.5$ and $f_t = 0.01$ versus $f_n = 0.5$ and an artificial coefficient 0.91 times (13)

stop mode, the initial motor velocity ω_0 and the time t_f are given.

The above problem is to find the optimal control i_a that minimizes the cost function for the given constrains. The cost function is the integrals of the total electrical energy

$$\min E_{in} = \int_0^{t_f} V_{1,a} i_{1,a} dt \tag{17}$$

with the constrains

$$\dot{\omega}_{1,m} = -A\omega_{1,m} + Bi_{1,a} + C$$

The Hamiltonian is formed by

$$H = (R_a i_{1,a} + K_e \omega_{1,m}) i_{1,a} + \lambda_1 \left(-A\omega_{1,m} + Bi_{1,a}\right) \tag{18}$$

with the costate equation as

$$\dot{\lambda}_1 = -\frac{\partial H}{\partial \omega_{1,m}} \tag{19}$$

where the subscript 1 represents the corresponding variations of the cruise start/stop mode. The optimal control is obtained by

$$\left.\frac{\partial H}{\partial i_{1,a}}\right|_{i_{1,a}=i^*_{1,a}} = 0 \tag{20}$$

and solving for $i^*_{1,a}$

$$i^*_{1,a} = \frac{-1}{2R_a}\left(\lambda_1 B + K_e \omega_{1,m}\right) \tag{21}$$

Solve the differential equations, and the optimal velocity is formulated by

$$\omega_{1,m}(t) = C_{11} e^{t/\tau_m} + C_{12} e^{-t/\tau_m} + F_{0,1} \tag{22}$$

$\tau_m = \sqrt{A^2 + ABK_e/R_a}^{-1}, F_{0,1} = -(2ACR_a + CBK_e)/2R_a$ where C_{11} and C_{12} are constants that are determined by the boundary conditions, and τ_m represents the mechanical time constant. The boundary condition of cruise start mode is $\omega_{1,m}(0) = 0, \omega_{1,m}(t_f) = \omega_f$. Then C_{11} and C_{12} in this condition are

$$\begin{aligned} C_{11} &= \frac{\omega_f + F_{0,1}\left(e^{-t_f/\tau_m} - 1\right)}{e^{t_f/\tau_m} - e^{-t_f/\tau_m}} \\ C_{12} &= \frac{-\omega_f - F_{0,1}\left(e^{t_f/\tau_m} - 1\right)}{e^{t_f/\tau_m} - e^{-t_f/\tau_m}} \end{aligned} \tag{23}$$

While the boundary condition of the cruise stop mode is $\omega_{1,m}(0) = \omega_0, \omega_{1,m}(t_f) = 0$, then, C_{11} and C_{12} are

$$\begin{aligned} C_{11} &= \frac{-\omega_0 e^{-t_f/\tau_m} - F_{0,1}\left(1 - e^{-t_f/\tau_m}\right)}{e^{t_f/\tau_m} - e^{-t_f/\tau_m}} \\ C_{12} &= \frac{\omega_0 e^{t_f/\tau_m} - F_{0,1}\left(e^{t_f/\tau_m} - 1\right)}{e^{t_f/\tau_m} - e^{-t_f/\tau_m}} \end{aligned} \tag{24}$$

The optimal velocity profile of the cruise start/stop mode is derived. Moreover, the optimal control $i^*_{1,a}$ is given by

$$i^*_{1,a} = B^{-1}(\dot{\omega}_m + A\omega_m - C) \tag{25}$$

Location mode

Since many segments of the pipe have been checked and do not need to be checked again, the robot needs position to position control. Under the location mode, the operator inputs the desired displacement S_f that the robot will move and the time t_f that robot will cost. Similarly, the cost function is also the instantaneous total electrical power

$$\min E_{in} = \int_0^{t_f} V_{2,a} i_{2,a} dt \tag{26}$$

with the constrains

$$\dot{\theta}_{2,m} = \omega_{2,m} \tag{27}$$

$$\dot{\omega}_{2,m} = -A\omega_{2,m} + Bi_{2,a} + C \tag{28}$$

The Hamiltonian is

$$H = \left(R_a i_{2,a} + K_e \omega_{2,m}\right) i_{2,a} + \lambda_{2,1}\omega_m - \lambda_{2,2}\left(A\omega_{2,m} - Bi_{2,a}\right) \tag{29}$$

Similarly procedure is adopted to get the optimal control, and the costate equations are

$$\dot{\lambda}_{2,1} = -\frac{\partial H}{\partial \theta_{2,m}} = 0 \tag{30}$$

$$\dot{\lambda}_{2,2} = -\frac{\partial H}{\partial \omega_{2,m}} \tag{31}$$

The optimal control $i^*_{2,a}$ is derived also by setting the partial differential equation to zero; thus

$$i^*_{2,a} = \frac{-1}{2R_a}\left(\lambda_{2,2} B + K_e \omega_{2,m}\right) \tag{32}$$

while the subscript 2 denotes the corresponding variations of the location mode to distinguish the cruise start/stop mode. The boundary conditions of location mode are $\omega_{2,m}(0) = \omega_{2,m}(t_f) = 0, S(t_f) = S_f, S(t_f) = S_f$. The relation between the rotational angle of the motor θ_f and the translational displacement of the robot S_f is

$$\theta_f = \int_0^{t_f} \omega_{2,m} dt = S_f i_{total}/\gamma \tag{33}$$

Then, the optimal velocity is obtained by solving the above equations and the boundary conditions

$$\omega_m(t) = C_1 e^{t/\tau_m} + C_2 e^{-t/\tau_m} + F_0 \tag{34}$$

$$C_1 = \frac{e^{-t_f/\tau_m} - 1}{e^{t_f/\tau_m} - e^{-t_f/\tau_m}} F_0$$

$$C_2 = \frac{1 - e^{t_f/\tau_m}}{e^{t_f/\tau_m} - e^{-t_f/\tau_m}} F_0$$

$$F_0 = \frac{S_f i_{total}\left(e^{t_f/\tau_m} - e^{-t_f/\tau_m}\right)}{\gamma\left(t_f\left(e^{t_f/\tau_m} - e^{-t_f/\tau_m}\right) + 2\tau_m\left(2 - e^{-t_f/\tau_m} - e^{t_f/\tau_m}\right)\right)}$$

$$\tau_m = \sqrt{A^2 + ABK_e/R_a}^{-1}$$

here, C_1, C_2 and F_0 are decided by the initial boundary conditions, and τ_m is the mechanical time constant. The optimal control $i^*_{2,a}$ can be also calculated from (25). Let $a = t_f/\tau_m$, and $\tau_1 = t/t_f$ be the reference time, and (34) can be reformed as

$$\omega_{2,m}(t) = \frac{S_f i_{total}}{\gamma t_f} a \frac{\sinh(a) - \sinh(a - \tau_1 a) - \sinh(\tau_1 a)}{a\sinh(a) - 2\cosh(a) + 2} \tag{35}$$

Trzynadlowski had discussed the optimal velocity by plotting a figure [12]. We will find the extremum of the velocity analytically. When $a \to +0$, by using the infinite series expansion e^a, (35) yields

$$\lim_{a\to 0} \omega_{2,m} = \frac{6\theta_f}{t_f}\left(\tau_1 - \tau_1^2\right) \tag{36}$$

and when $a \to +\infty$, (35) yields

$$\lim_{a\to +\infty} \omega_{2,m} = \frac{S_f i_{total}}{\gamma t_f} \tag{37}$$

(36) and (37) can be explained as two extreme conditions for a certain system whose mechanical time constant τ_m has been decided. Assume S_f keeps constant, and the final time t_f varies. When t_f is too short with respect to τ_m, the velocity profile will approach (36), but if t_f is too long with respect to τ_m, the velocity profile is getting close to (37). For better understanding, let $\omega_m/(\theta_f/t_f)$ be the reference velocity and t/t_f be the reference time, and when $a = t_f/\tau_m$ varies, Fig. 7 is plotted as velocity per unit versus time per unit by using the parameters of Table 1.

Velocity constrains

It is known that each motor has its maximum speed limit; moreover, it also has a maximum continuous working speed $\omega_{m,r}$ for practical use. Let k_v be the speed ratio and defined as

$$k_v = \frac{\omega_{m,r}\gamma t_f}{i_{total} S_f} \tag{38}$$

From the above discussion, we will get $1 \le k_v \le 1.5$. Thus, when k_v is not belonging to this interval, then we need to formulate a new velocity profile. Because $k_v = 1.5$, the velocity profile becomes parabola as indicated in (36), and we still adopt this parabolic curve as the velocity profile when $k_v \ge 1.5$. Then, the velocity becomes

$$\omega_m(t) = \frac{6 S_f i_{total}}{\gamma t_f}\left(t/t_f - t^2/t_f^2\right) \tag{39}$$

As for the condition $0 < k_v < 1$, it means that the average speed $S_f i_{total}/\gamma t_f$ that is given by operator has exceeded the maximum continuous working speed $\omega_{m,r}$. Thus, the robot cannot move a displacement S_f within time t_f. Generally, S_f is the destination and cannot change, and the other way is to adjust the time t_f. From Fig. 7, we can see the region of this condition lies beneath the trapezoidal speed profile and we just follow this trend to form the velocity profile, which is

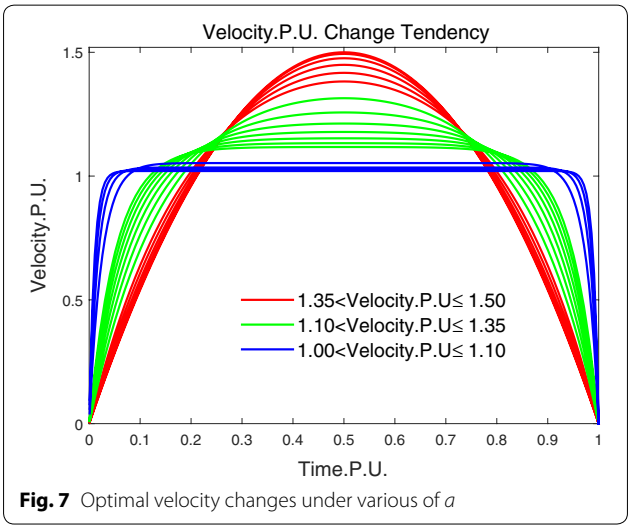

Fig. 7 Optimal velocity changes under various of *a*

Table 1 Parameters of the robot and motor [13]

Parameter	Value	Parameter	Value
P	20 W (rated)	D	0.19 m
K_t	0.0170 N m/A	α	15°
K_e	0.0170 V s/rad	T_{load}	0.3 N m
R_a	1.17 Ω	J_{eq}	4×10^{-5} kg m^2
R_h	212.6 Ω	total	111
$30\omega_{m,r}/\pi$	6000 rpm	c_m	2×10^{-5} N m s/rad

$$\omega_{\mathrm{m}}(t) = \begin{cases} \omega_{\mathrm{m,r}} - 4\omega_{\mathrm{m,r}}(t/t_1 - 0.5)^2 & 0 \le t \le 0.5t_1 \\ \omega_{\mathrm{m,r}} & 0.5t_1 < t \le t_{\mathrm{f}} - 0.5t_1 \\ \omega_{\mathrm{m,r}} - 4\omega_{\mathrm{m,r}}((t - t_{\mathrm{f}})/t_1 + 0.5)^2 & (t_{\mathrm{f}} - 0.5t_1) < t \le t_{\mathrm{f}} \end{cases} \tag{40}$$

Between $[0, 0.5t_1]$ the motor is accelerating the robot along the parabolic curve to the maximum continuous working speed of $\omega_{\mathrm{m,r}}$, then it moves at this speed for a while, and finally, it begins to decelerate the robot along the parabolic curve to complete the desired displacement. And t_1 and t_{f} can be derived by minimizing the total energy E_{in} with respect to the time t

$$S_{\mathrm{f}} = \frac{\gamma}{i_{\mathrm{total}}} \int_0^{t_{\mathrm{f}}} \omega_{\mathrm{m,r}} \mathrm{d}t \tag{41}$$

$$E_{\mathrm{in}} = \int_0^{0.5t_1} V_{\mathrm{a}} i_{\mathrm{a}} \mathrm{d}t + \int_{\tau_1 t_1}^{t_{\mathrm{t}} - 0.5t_1} V_{\mathrm{a}} i_{\mathrm{a}} \mathrm{d}t + \int_{t_{\mathrm{f}} - 0.5t_1}^{t_{\mathrm{f}}} V_{\mathrm{a}} i_{\mathrm{a}} \mathrm{d}t \tag{42}$$

After discussing the above working conditions of the robot, we can formulate the optimal velocity selection strategy, which considers the velocity constrains, under location mode

$$\omega_{\mathrm{m}}(t) = \begin{cases} \text{Equation (40)} & 0 \le k_{\mathrm{v}} < 1 \\ \text{Equation (34)} & 1 \le k_{\mathrm{v}} \le 1.5 \\ \text{Equation (39)} & 1.5 < k_{\mathrm{v}} \end{cases} \tag{43}$$

Equation (43) guarantees the motor and the robot working in a continuous and safe region, and it is suitable for the pipe robot which will work in field environment. Judging maximum velocity problem does not exist in the cruise start/stop mode, because the control system will compare the input speed ω_{f} with $\omega_{\mathrm{m,r}}$ directly and inform the operator to change the velocity, if ω_{f} is larger than $\omega_{\mathrm{m,r}}$.

Results and discussion

We have derived the energy-efficient control laws of the robot in cruise start/stop mode and location mode, respectively. In this section, simulations are performed to evaluate the proposed energy-efficient control law, and these results are compared with two benchmark methods. One is sinusoidal velocity function based on the computed torque control and is given by

$$S(t) = \frac{S_{\mathrm{f}}}{2}\left(1 - \cos\left(\pi \frac{t}{t_{\mathrm{f}}}\right)\right) \tag{44}$$

$$\omega(t) = \frac{\pi S_{\mathrm{f}}}{2\gamma t_{\mathrm{f}}} \sin\left(\pi \frac{t}{t_{\mathrm{f}}}\right) \tag{45}$$

The second benchmark method is the loss minimization control method that optimizes the armature loss $i_{\mathrm{a}}^2 R_{\mathrm{a}}$ of the DC motor, which only considered R_{a}.

Figure 8 shows the results of the two methods within the same time interval to reach a same speed that the operator inputs. The velocity and energy dissipation of minimum energy control are both lower than that of loss minimization control that only considers R_{a}. Figure 8c shows the two conditions after the robot reached the speed of the cruise start mode: One is that the robot keeps the velocity constant, and the other is that the robot's speed varies (we use a sinusoidal function in this figure). Figure 8d shows that the velocity variation needs more energy to keep the robot moving than that of keeping the velocity invariable. Thus, it is better to keep the speed of the robot stable in the pipe in order to save energy in the field environments.

In Fig. 9a the velocity of the minimum energy control is the lowest one, compared to that of the other two, whose speed exceeds the maximum continuous working speed 0.144 m/s for a short while. Figure 9a, c also shows that the speed of minimum energy control accelerates and decelerates rapidly and maintains a stable speed; this is convenient for the robot while checking the pipe, because a stable moving speed is reasonable for sensor to collect data; as for the other two methods, the speed varies during the whole operation time.

Figure 10a shows the energy dissipation of location mode in Fig. 9. The sinusoidal control causes the highest energy, while the loss minimization cost is the lowest. This is because in minimum energy control method, we have considered the armature resistance R_{a} and the equivalent resistance R_{h} of the power loss due to the air resistance of the rotor and power loss due to friction between the mechanical parts as shown in Fig. 3. Thus, the armature current is larger than that of only considering R_{a}, when the robot works at the same combination of torque and velocity, which causes more electrical energy. Figure 10b is the condition that $R_{\mathrm{h}} \to \infty$, and the result shows the minimum energy control cost is the lowest energy. Therefore, when we consider R_{h}, the total input energy will increase and may possibly greater than loss minimization control, but it gives a more accurate model and numerical results than that of only considering the armature resistance (see Table 2).

Figure 11 shows the velocity selection strategy according to the value of k_{v}. When the value of k_{v} is greater than 1.5, the parabolic curve is selected as the velocity profile since it is the upper limit of the velocity per unit (see Fig. 7). While the value of k_{v} is lower than 1, which means

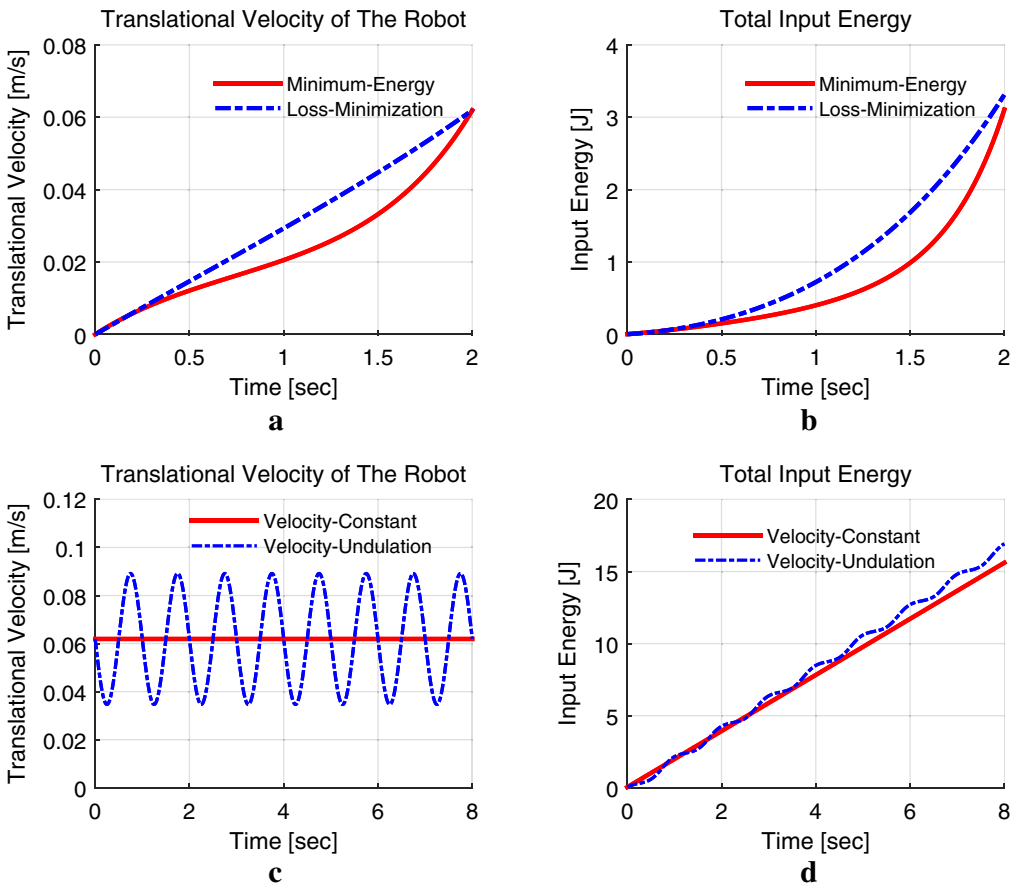

Fig. 8 Cruise start mode with $\omega_f = 270$ rad/s, $t_f = 2$ s. **a** Velocity comparison, **b** energy dissipation, **c** velocity constant versus velocity undulation, **d** energy dissipation

even the maximum speed of motor does not satisfy the requirement of S_f and t_f, the velocity is generated according to (40), which minimizes the total energy as well. From the above, we can see that the minimum energy control causes lower energy dissipation and provides more accurate numerical results, compared to that of the loss minimization control only considering armature resistance. The summary of energy dissipations is listed in Table 2.

Conclusion

This paper considers a more accurate motor model and uses total input energy as the cost function to generate energy-efficient control laws for a pipe inspection robot. This pipe robot has two working modes: driving mode and detecting mode. Robot needs to keep a speed to move or move a distance to check the pipe; thus, we propose two types control: One is cruise start/stop control, and the other is location control. For the cruise mode and location mode, we have derived the optimal velocity and propose a velocity selection strategy according to the k_v. This velocity selection strategy can guarantee the motor work in safe region, which also means decreasing the total input energy consumption, and can treat all the combinations of the S_f and t_f. Results show that this method indeed saves the energy dissipation with the commonly used method, and provide more accurate model compared with the loss minimization control.

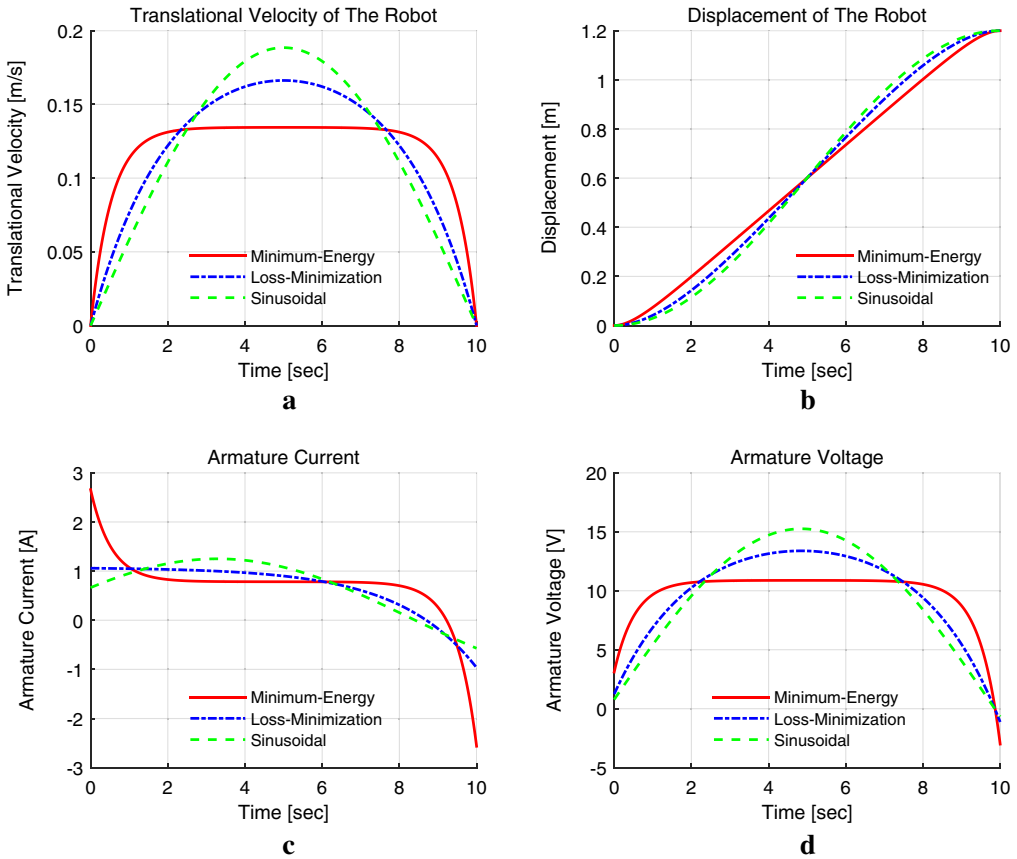

Fig. 9 Location mode with $S_f = 1.2\,\text{m}, t_f = 10\,\text{s}$ with $k_v = 1.20$. **a** Translational velocity, **b** displacement, **c** armature current, **d** armature voltage

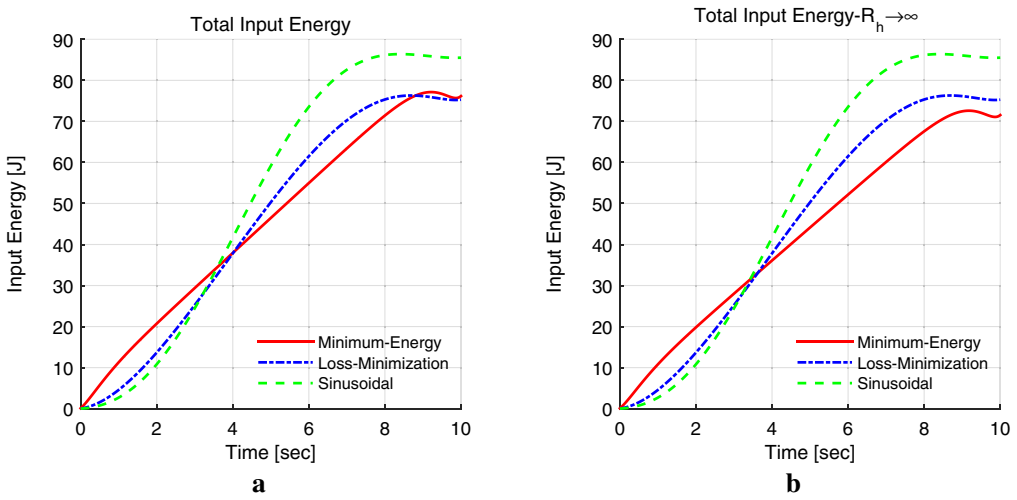

Fig. 10 Results of the total energy consumption. **a** Results considering R_a and R_h, **b** results of $R_h \to \infty$ (only considering R_a)

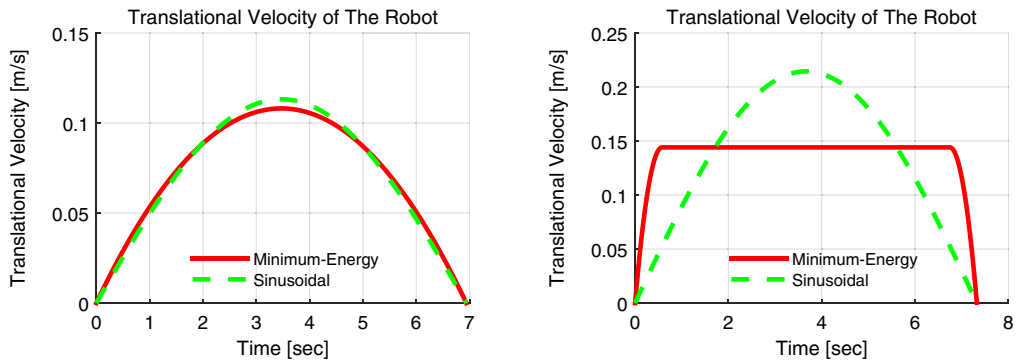

Fig. 11 Velocity selection according to k_v. **a** Velocity profiles under $S_f = 0.5$ m, $t_f = 6.94$ s, and $k_v = 2$, **b** velocity profiles under the required $S_f = 1$m and $t_f = 1$s that means $k_v < 1$, thus, the recalculated time $t_f = 7.33$ s and $t_1 = 1.16$ s

Table 2 Summary of total input energy

S_f (m)	t_f (s)	I: $\int_0^{t_f} V_a i_a dt$	II: $\int_0^{t_f} i_a^2 R_a dt$	III: $\int_0^{t_f} V_a i_a dt$
0.3 m	4	14.79 (14.02)	14.37	15.65
1.2 m	10	76.09 (71.46)	75.28	85.53
2.0 m	15	134.91 (126.50)	132.83	155.18
Figure 8b		3.10	3.31	14.12
Figure 11a		23.30 (19.70)	21.65	23.91
Figure 11b		83.82	N/A	86.40

I refers to the minimum energy control that considers R_a and R_h, while the numbers in the bracket denote the results that $R_h \to \infty$; *II* refers to the loss minimization control that only considers R_a; *III* refers to the computed torque control that considers R_a and R_h

Received: 20 April 2016 Accepted: 27 June 2016
Published online: 11 July 2016

Authors' contributions

A energy-efficient control law is proposed for a pipe robot by considering the characteristics of motor. Optimal velocity profiles are derived from two sets of boundary conditions. A velocity selection strategy is generated by considering the capacity of motor. All authors read and approved the final manuscript.

Author details

[1] School of Mechanical Engineering and Automation, Harbin Institute of Technology Shenzhen Graduate School, ShenZhen 518055, China. [2] Department of Mechanical and Automation Engineering, The Chinese University of Hong Kong, Shatin, Hong Kong, China. [3] Shenyang Institute of Automation, Chinese Academy of Sciences, Shenyang 110016, China. [4] Department of Robotics, Ritsumeikan University, Shiga-ken 525-8577, Japan.

Acknowledgements

The authors would like to thank Dr. Rongchuan Sun for his help in programming. The work is a part supported by Shenzhen Peacock Plan Team Grant (KQTD20140630150243062), Shenzhen Key Laboratory Grant (ZDSYS201405081618 25065), the Hong Kong Research Grants Council (CUHK6/CRF/13G) and the Hong Kong Innovation and Technology Fund (ITS/112/15F).

Competing interests

The authors declare that they have no competing interests.

References

1. Roh SG, Choi HR. Differential-drive in-pipe robot for moving inside urban gas pipelines. IEEE Trans Robot. 2005;21(1):1–17.
2. Oya T, Okada T. Development of a steerable, wheel-type, in-pipe robot and its path planning. Adv Robot. 2005;19(6):635–50.
3. Horodinca M, Doroftei I, Mignon E, Preumont A. A simple architecture for in-pipe inspection robots. In: International colloquium on autonomous and mobile systems; 2002.
4. Li P, Ma S, Li B, Wang Y. Design of a mobile mechanism possessing driving ability and detecting function for in-pipe inspection. In: Proceedings—IEEE international conference on robotics and automation; 2008. p. 3992–97
5. Paes K, Dewulf W, Elst KV, Kellens K, Slaets P. Energy efficient trajectories for an industrial ABB robot. Proc CIRP. 2014;15:105–10.
6. Aghili F. Energy-efficient and fault-tolerant control of multiphase nonsinusoidal pm synchronous machines. IEEE/ASME Trans Mechatron. 2015;20(6):2736–51.
7. Kusko A, Galler D. Control means for minimization of losses in ac and dc motor drives. IEEE Trans Ind Appl. 1983;ia-19(4):561–70.
8. Egami T, Tsuchiya T. Efficiency optimized speed-control system based on improved optimal regulator theory. IEEE Trans Ind Electron. 1986;IE-33(2):114–25.
9. Egami T, Morita H, Tsuchiya T. Efficiency optimized model reference adaptive control system for a DC motor. IEEE Trans Ind Electron. 1990;37(1):28–33.
10. Margaris N, Goutas T, Doulgeri Z, Paschali A. Loss minimization in DC drives. IEEE Trans Ind Electron. 1991;38(5):328–36.
11. Ma S. Time-optimal control of robotic manipulators with limit heat characteristics of the actuator. Adv Robot. 2002;16(4):309–24.
12. Trzynadlowski AM. Energy optimization of a certain class of incremental motion DC drives. IEEE Trans Ind Electron. 1988;35(1):60–6.
13. Maxon motor catalog. http://www.maxonmotor.com/maxon/view/catalog/